

Ferroc quadrupolar ordering in CeCoSi revealed using ^{59}Co -NMR measurements

Masahiro Manago,^{1,*} Ayano Ishigaki,² Hideki Tou,² Hisatomo Harima,² Hiroshi Tanida,³ and Hisashi Kotegawa²

¹*Department of Applied Physics, Shimane University, Matsue 690-8504, Japan*

²*Department of Physics, Kobe University, Kobe 657-8501, Japan*

³*Liberal Arts and Sciences, Toyama Prefectural University, Imizu, Toyama 939-0398, Japan*

A nonmagnetic phase transition at $T_0 \sim 12$ K in the tetragonal system CeCoSi with a Kramers doublet ground state is reminiscent of an electric quadrupole ordering, even though its well-separated crystal-electric-field (CEF) levels are unlikely to acquire higher-order multipole degrees of freedom. Here, we report ^{59}Co nuclear magnetic resonance (NMR) studies that are highly compatible with a ferroic quadrupole ordering below T_0 . Changes in the NMR spectra below T_0 suggest that an external magnetic field induces ferroic Ce dipole moments orthogonal to the field, enabling domain selection in the nonmagnetic phase. Our findings suggest the presence of a ferroic O_{zx} -type quadrupole component in CeCoSi and demonstrate that quadrupole ordering may occur under well-separated CEF levels in tetragonal systems.

I. INTRODUCTION

Order parameters in phase transitions are determined through crystal symmetries and interactions. In f -electron systems, the degrees of freedom of unpaired electrons are strongly affected by spin-orbit coupling, but ultimately, the crystal electric field (CEF) determines their ground state. If a CEF ground state is a Kramers doublet, the f -electron degrees of freedom are limited to a magnetic origin unless the excited states are located closely¹⁻⁶. This restriction is modified by the hybridization between the conduction electrons and the f -electrons (c - f hybridization); Kondo lattice systems that have the Kramers doublet as their ground state have a chance to acquire higher-order multipole degrees of freedom owing to the contribution of the CEF excited states. A rare example of this is CeTe⁷. Although CeTe is a cubic system, the CEF ground state is a Kramers doublet, and the separation between the ground state and the excited state is $\Delta \sim 30$ K. Under pressure, the enhanced Kondo effect induces an electric quadrupole ordering, even though Δ is one order larger than the quadrupole ordering temperature. Another possible example has been recently demonstrated in the tetragonal system CeRh₂As₂ with the Kramers doublet ground state^{8,9}. A quadrupole-density-wave state below 0.4 K has been proposed, although $\Delta \sim 30$ K is two orders larger than the ordering temperature. In CeRh₂As₂ and CeTe, the Kondo temperatures T_K are comparable to Δ , indicating the sufficient mixing of two CEF levels.

Here, we focus on the tetragonal system CeCoSi, in which quadrupole ordering has been proposed^{10,11}. In CeCoSi, aside from the antiferromagnetic transition at Néel temperature $T_N = 9.4$ K, another phase transition was initially observed under pressure; the transition temperature of $T_0 = 38$ K at 1.5 GPa¹². This was later also confirmed at ambient pressure at $T_0 = 12$ K¹¹. The increase in T_0 under the magnetic field was reminiscent of the quadrupole ordering¹¹, whereas Δ is ~ 125 K¹³. This value is much higher than those reported for CeTe and CeRh₂As₂ and comparable to that of the prototype Ce-based tetragonal system CeCu₂Si₂ ($\Delta \sim 140$ K)¹⁴, where quadrupole degrees of freedom have been inconsiderable. Although interorbital interactions between the ground and excited states can induce quadrupole orderings phenomenolog-

ically even with such a large Δ ¹⁵, their feasibility remains an open question.

Our previous ^{59}Co -nuclear magnetic resonance (NMR) and nuclear quadrupole resonance (NQR) measurements in CeCoSi show the symmetry breaking of a nonmagnetic origin below T_0 ¹⁶. The splitting of the NMR spectrum suggested the emergence of the field-induced dipole moments, which are characteristic in quadrupole ordering states¹⁷⁻²⁰. However, the combined results of NMR and NQR did not reveal the order parameter. A recent high-resolution x-ray diffraction (XRD) measurement has clearly revealed the triclinic distortion below T_{s1} , which is considered the same as T_0 at zero field²¹. The triclinic angles are $\alpha = \beta = 89.64^\circ$ and $\gamma \simeq 90^\circ$ at 10 K. If we recognize it as the quadrupole ordering, this distortion is compatible with a ferroic $O_{yz} + O_{zx}$ -type ordering. The interpretation of the previous NMR study was inconsistent with this ferroic ordering because the splitting of the spectrum was reminiscent of antiferroic ordering. Solving this inconsistency is essential to understand the nature of the nonmagnetic ordered phase in CeCoSi.

In this article, we present field-angle-controlled NMR spectra measured at ambient pressure on a CeCoSi single crystal. In the nonmagnetic ordered state, we found that one of the split NMR peaks became predominant as tilting the external magnetic field from the in-plane direction. This suggests that the splitting arises not from the emergence of inequivalent Co sites in a unit cell but from different domains of a ferroic ordered state. The results of this study eliminate the inconsistency between XRD and the previous NMR findings, being very compatible with the presence of a ferroic O_{zx} quadrupole component below T_0 .

II. EXPERIMENTAL

A plate-shaped single-crystalline CeCoSi sample (4 mm \times 2 mm \times 0.4 mm) was grown using the Ce/Co eutectic flux method, as described in Ref. 11. ^{59}Co (nuclear spin $I = 7/2$) NMR measurements were performed at ambient pressure and a temperature range of 10–20 K above T_N . NMR spectra were measured in several field directions controlled by a home made double-axis rotator. The field angle was evaluated from

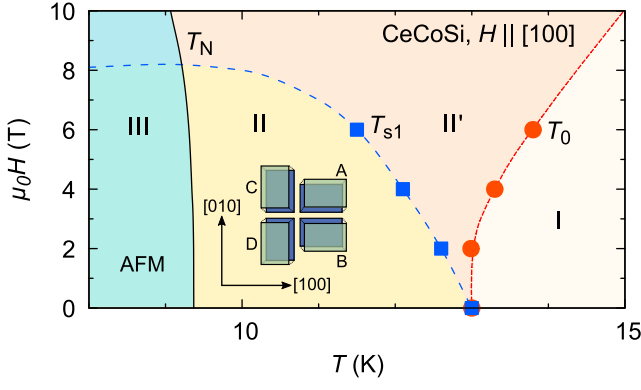


FIG. 1. Field–temperature phase diagram of CeCoSi along the [100] direction. The transition temperatures T_0 and T_{s1} and the Néel temperature T_N were from literature^{11,21}. Phases II and II' represent the nonmagnetic ordered states. The crystal symmetry is lowered from tetragonal (phase I) to triclinic (phase II), and that in phase II' remains unclear. The inset shows four domains for the triclinic distortion below T_{s1} ²¹.

the NMR frequencies above T_0 . The angle precision is $\sim 0.1^\circ$ for the polar angle θ and $\sim 5^\circ$ for the azimuth angle ϕ . The electric field gradient (EFG) parameters, i.e, the quadrupole frequency ν_Q and the asymmetry parameter η , were deduced from the NQR results¹⁶ (see also the Appendix) and fixed in the analysis of the NMR spectra. The EFG at the Co site was calculated through a full-potential linear augmented plane wave (LAPW) calculation within the local density approximation (LDA).

III. RESULTS AND DISCUSSION

First, we show the field–temperature phase diagram in Fig. 1, which was revealed by XRD²¹ and confirmed by bulk measurements²². Here, T_0 increased by applying the external field along the [100] direction, while the structural transition temperature T_{s1} decreased. The separation of T_0 and T_{s1} suggests multiple components of the order parameter. The inset shows the four domains (A–D) in the triclinic symmetry confirmed in phase II²¹, while a change in the structural symmetry in phase II' is undetected at the moment.

The Co site in CeCoSi is surrounded by the four nearest Ce atoms, forming a tetrahedron, as shown in Fig. 2(a). The local symmetry is $4m2$ above T_0 , ensuring a single site in the NMR spectrum for any field directions. In this symmetry, the maximum principal axis of the EFG, V_{zz} , is directed along the [001] direction at the Co site. The field-angle dependence of the NMR spectra at the third satellite peak ($7/2 \leftrightarrow 5/2$ transition) is shown in Fig. 3(a). The measurements at 10 K were performed in phase II, where the four domains were formed. The direction of the magnetic field varied from [100] to [001]. Here, θ_0 is the angle between the external magnetic field, H_{ext} , and the [001] direction in the tetragonal symmetry. At 10 K, when θ_0 was slightly changed from 90° , the peak splitting occurred due to the symmetry lowering below T_0 ¹⁶. With fur-

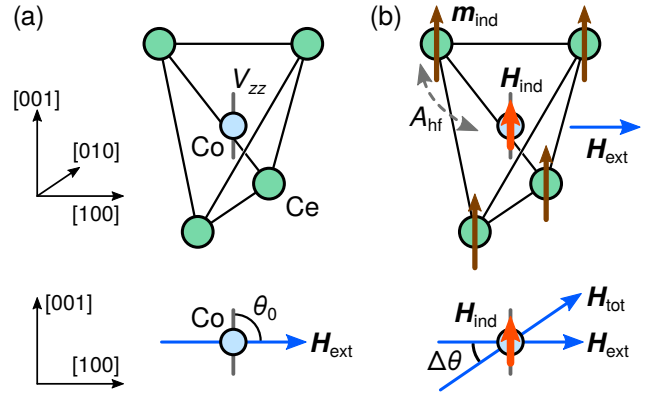


FIG. 2. The arrangement of the NMR measurement for CeCoSi. (a) A Co site surrounded by four Ce atoms forming a tetrahedron. The maximum principal axis of the EFG, V_{zz} , is parallel to the [001] direction. The bottom figure shows the magnetic field direction θ_0 from [001]. (b) Below T_0 , induced moments at the Ce sites m_{ind} emerge perpendicular to the external field. The magnetic field at the Co site H_{ind} is induced through the hyperfine coupling. Only the perpendicular component of the Ce moment is shown. The bottom figure shows the change in the field angle $\Delta\theta$ due to the emergence of H_{ind} .

ther tilting, the intensity of the lower-frequency peak became weaker and almost disappeared at $\theta_0 \lesssim 80^\circ$. This strongly suggests that the NMR splitting arises not from the emergence of inequivalent Co sites in a unit cell but from a difference in the resonance condition among the domains; the Co site remained equivalent in each domain, and some of the A–D domains were selected by the c -axis component of the magnetic field. Similar results were obtained between the [110] and [001] directions, as shown in Fig. 3(b). Two peaks were observed when the magnetic field was tilted slightly from the [110] direction. These correspond to the domains A and D because the XRD study clarified the domain selection by the in-plane field along the [110] direction²¹. The NMR results revealed further domain selection induced by the out-of-plane field at $\theta_0 \lesssim 80^\circ$.

Figures 3(c) and 3(d) show the field-angle dependence of the peak frequencies at 10 K. The results are symmetrized with respect to $\theta_0 = 90^\circ$. They are reproduced by

$$f = \gamma H_{\text{ext}} [1 + K(\theta_0)] + \frac{3}{2} \nu_Q (3 \cos^2 \theta - 1), \quad (1)$$

which is obtained within the first-order perturbation with respect to the quadrupolar frequency ν_Q , where γ is a gyromagnetic ratio, $K(\theta_0)$ is the Knight shift, and θ is the angle between the total magnetic field, H_{total} , at the Co site and the direction of V_{zz} . Above T_0 , θ is equal to θ_0 determined by H_{ext} , and the frequency achieves its minimum at $\theta_0 = \theta = 90^\circ$. The symmetry reduction below T_0 causes a difference between θ_0 and θ , which is denoted as $\theta = \theta_0 \pm \Delta\theta$. The best fit was obtained with a tilting angle of $\Delta\theta \simeq 2\text{--}3^\circ$. This means that the NMR splitting is due to the change in the angle between H_{total} and the V_{zz} ¹⁶.

We carefully checked the possibility that $\Delta\theta$ mainly arises

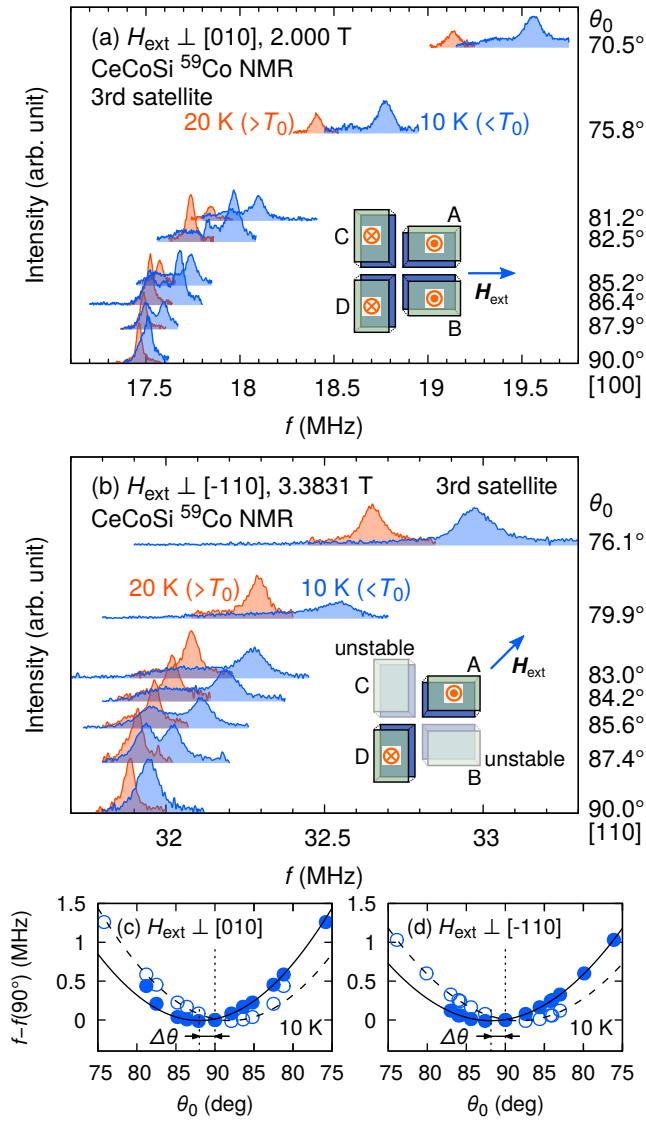


FIG. 3. (a) Field-angle dependence of the ^{59}Co NMR third satellite spectra of CeCoSi at 10 and 20 K with θ_0 from [001] to the [100] axis at 2.000 T. The inset represents the induced field directions shown in red for each domain. (b) Field-angle dependence between [110] and [001] directions at 3.3831 T. Some domains are unstable for the in-plane field. In both cases, the domain selection occurs in the out-of-plane field. (c), (d) Field angle dependence of the resonant frequencies at 10 K for (c) $H \perp [010]$ and (d) $H \perp [\bar{1}10]$. The solid and dashed lines show the best fit of the result with $\frac{9}{2}v_Q \cos^2(\theta_0 \pm \Delta\theta)$.

from the tilting of V_{zz} due to the triclinic distortion. Thus, the changes in the EFG parameters were obtained through the band-structure calculation using structural parameters in triclinic symmetry²¹. The calculation provided the result that the tilting of V_{zz} is 0.16° , one order smaller than the experimental $\Delta\theta$. This suggests that the change in the EFG is very small in CeCoSi, and that nonzero $\Delta\theta$ arises from the tilting of H_{total} at the Co site. We investigated the breaking of the four-fold symmetry in the EFG using NQR measurements, but its change into the triclinic symmetry was undetected within the

experimental error, as shown in the Appendix. This is also consistent with the calculation showing a small change in the EFG.

This interpretation is also supported by the field-direction dependence of $\Delta\theta$ shown below. Figures 4(a)–4(c) show the temperature dependence of the NMR spectra in different fields. For the respective spectra, θ was evaluated for the high-frequency peak of the split peaks. The temperature dependence is shown in Figs. 4(d)–4(f). A clear kink corresponding to T_0 appears for all the field settings. T_0 increases as H_{ext} increases along the [100] direction, which is in good agreement with other experimental reports^{11,21,22}. T_0 in NMR is slightly higher than those in other reports, which is probably owing to the out-of-plane component of the H_{ext} . The temperature dependences of $\Delta\theta = |\theta_0 - \theta|$ are summarized in Fig. 4(g), where the temperatures are normalized by T_0 . The $\Delta\theta$ is almost in-

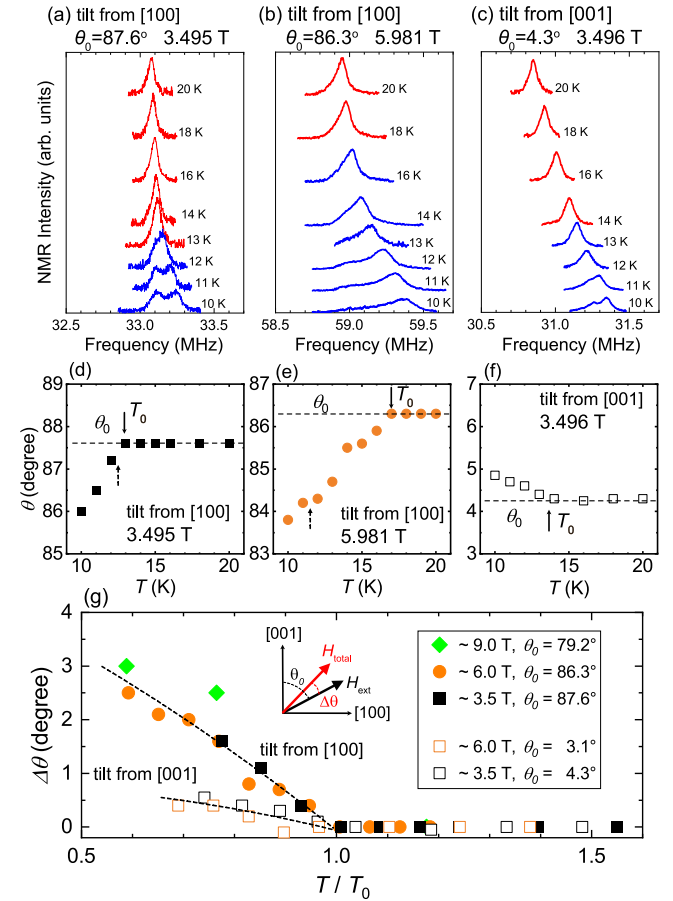


FIG. 4. (a)–(c) Temperature dependence of the ^{59}Co NMR third satellite peaks: (a) 3.495 T with $\theta_0 = 87.6^\circ$, (b) 5.981 T with $\theta_0 = 86.3^\circ$ and (c) 3.496 T with $\theta_0 = 4.3^\circ$. The spectra are vertically shifted for clarity. (d)–(f) Temperature dependence of the angle θ of ^{59}Co NMR spectra in several fields. The horizontal dashed lines represent the external field angle θ_0 . The solid arrows indicate T_0 determined in NMR, while the dotted arrows are T_{s1} ²¹. (g) Temperature dependence of the tilting angle $\Delta\theta$ of ^{59}Co NMR spectra in several fields. The temperature is normalized by T_0 for each field. The dotted curves are guides for the eye.

dependent of the strength of H_{ext} for each field direction. At $T/T_0 \approx 0.7$, $\Delta\theta$ for H_{ext} tilted from [100] is approximately four times larger than that for H_{ext} tilted from [001]. The origin of $\Delta\theta$ cannot be explained solely by the tilting of the V_{zz} originating in the structural distortion because it must provide the same $\Delta\theta$ in any field directions, clearly indicating that $\Delta\theta$ is dominated by the tilting of H_{total} .

As shown in Fig. 2(b), the tilting of H_{total} arises from the emergence of the H_{ind} at the Co site, which is orthogonal to the H_{ext} . Because $H_{\text{ind}}/H_{\text{ext}} \approx \tan(\Delta\theta)$, the field-independent $\Delta\theta$ indicates that H_{ind} is almost proportional to H_{ext} . The observations of the peaks assigned to the single Co site in NMR at $\theta_0 \lesssim 80^\circ$ suggest that the H_{ind} is uniform at the Co nuclei in a domain; therefore, the Ce local moments should be uniform below T_0 . In this case, the hyperfine field at the Co site is dominated by a diagonal part¹⁶ (see also the Appendix); that is, the H_{ind} at the Co site is induced by the Ce moments parallel to them, as shown in Fig. 2(b). In the case of $H_{\text{ext}} \parallel [100]$, the orthogonal H_{ind} along the [001] direction is considered to arise from $A_{cc}m_{\text{ind}}^c$, where A_{ij} is a component of the hyperfine coupling tensor, and m_{ind}^i is the i -axis component of the induced Ce moment ($i, j = a, b$, and c). Likewise, in the case of $H_{\text{ext}} \parallel [001]$, the orthogonal H_{ind} is considered to arise from $A_{aa}m_{\text{ind}}^a$. Therefore, the H_{ext} induces the orthogonal Ce dipole moments. Experimentally, $\Delta\theta$ for the [100] direction is four times larger than that for the [001], as shown in Fig. 4(g). It arises from a difference between $A_{cc}m_{\text{ind}}^c$ and $A_{aa}m_{\text{ind}}^a$. Using $A_{cc} \sim 3 \text{ T}/\mu_{\text{B}}$ and $A_{aa} \sim 0.6 \text{ T}/\mu_{\text{B}}$ ¹⁶, anisotropy in the induced moments m_{ind}^c and m_{ind}^a is considered weak. It is possible to make a rough estimation of the orthogonal induced moment size using the relations of $H_{\text{ind}} = A_{ij}m_{\text{ind}}^i$ and $H_{\text{ind}}/H_{\text{ext}} \approx \tan(\Delta\theta)$. It yields

$$\frac{m_{\text{ind}}^c}{H_{\text{ext}}} \sim \frac{m_{\text{ind}}^a}{H_{\text{ext}}} \sim \frac{\tan(\Delta\theta)}{A_{ii}} \sim 0.01\mu_{\text{B}}/\text{T} \quad (2)$$

for $H_{\text{ext}} \parallel [100]$ and [001], respectively, when the tilting angle is $\Delta\theta \approx 2^\circ$ for $H_{\text{ext}} \parallel [100]$ and $\Delta\theta \approx 0.5^\circ$ for $H_{\text{ext}} \parallel [001]$. The Ce magnetic moment also possesses the component parallel to the external field, which is estimated from the Knight shift as

$$\frac{m_i}{H_{\text{ext}}} = \frac{K_i - K_i^{\text{orb}}}{A_{ii}}, \quad (3)$$

where K_i^{orb} is an orbital shift along the i direction. The moment is 0.025 and $0.030\mu_{\text{B}}/\text{T}$, for $H_{\text{ext}} \parallel [100]$ and [001], respectively, using the Knight shift values at 10 K ¹⁶. These values are also evaluated from a macroscopic magnetization¹¹. Note that the present NMR spectra were insensitive to the induced moment along the [010] direction for $H_{\text{ext}} \parallel [100]$, even if it exists.

The uniform and orthogonal m_{ind} at the Ce sites is compatible with ferroic O_{zx} -type quadrupole ordering among possible quadrupole order parameters summarized in the literature¹⁵. In this ordered state, the Ce dipole moment is fixed along the diagonal direction in the zx plane. The magnetic field along the [100] ([001]) direction induces the additional magnetic moment along the [001] ([100]) directions, respectively, consistent with our observations. As shown in Fig. 4(e), no clear

anomaly appeared at T_{s1} in NMR, suggesting that the order parameter emerging below T_{s1} is insensitive to Co-NMR for $H_{\text{ext}} \sim [100]$, which corresponds to O_{yz} . Therefore, it is suggested that phase II' is an O_{zx} ordered state and phase II is an $O_{yz} + O_{zx}$ ordered state. The latter gives the triclinic distortion, which is consistent with the XRD²¹. This is also consistent with the anisotropic phase diagram between $H \parallel [100]$ and $H \parallel [110]$ ²¹ because $H \parallel [100]$ lifts the degeneracy of O_{yz} and O_{zx} . Additionally, this order parameter completely explains the domain selection observed in NMR. When we applied the magnetic field along the [100] direction, m_{ind}^c was positive in the domains A ($O_{yz} + O_{zx}$) and B ($-O_{yz} + O_{zx}$), and negative in the domains C ($O_{yz} - O_{zx}$) and D ($-O_{yz} - O_{zx}$), as shown in Fig. 3(a). Tilting of the magnetic fields towards $\theta_0 < 80^\circ$ induces the positive c -axis component in the H_{ext} , stabilizing domains A and B. In the [110] direction, as shown in Fig. 3(b), m_{ind}^c is opposite between the domains A and D. The domain selection under the c -axis magnetic field also occurs when $H \parallel [001]$.

Ferroic O_{zx} ordering expected in phase II' should induce a monoclinic distortion. However, this has not been seen in the (207) reflection of XRD²¹. For a setting of the XRD measurement, the order parameter expected from NMR in phase II' is O_{yz} because the direction of H_{ext} was treated as [010]. In this situation, the domain formation by the monoclinic distortion does not cause the splitting of the (207) reflection because the mirror symmetry is not broken with respect to the yz plane. This might be why the structural change was not seen in the XRD measurement.

The NMR anomalies in the nonmagnetic ordered phase of CeCoSi are totally comprehended as ferroic quadrupole ordering. An open issue is the full understanding of the order parameter of this phase. While the present NMR revealed the existence of the O_{zx} component, the order parameter could be more complicated than the pure O_{zx} or $O_{yz} + O_{zx}$ state because of the low crystal symmetry, allowing multiple quadrupole components in the order parameter. The field-induced successive transitions along the [100] direction could be caused by the suppression of the O_{yz} component by the field, although this has not been directly confirmed yet. A full elucidation of the field-temperature phase diagram is important in CeCoSi.

A more fundamental issue is whether its emergence is possible under the CEF levels of $\Delta \sim 125 \text{ K}$ ¹³. Observing the situation under pressure, the difference between Δ and T_0 becomes smaller ($\Delta \sim 3T_0$) as T_0 increases to 38 K ¹². In TmAg₂, the quadrupole ordering occurs for $\Delta \sim 3T_0$ even though the c - f hybridization is weak³. Considering the Kondo effect is enhanced under pressure in CeCoSi^{10,12}, it is not an unrealistic condition for the occurrence of a quadrupole ordering, although a reason for the high T_0 is another problem. At ambient pressure, weaker c - f hybridization suppresses the interaction between the quadrupole moments and the quadrupole degrees of freedom. This is consistent with the weak anomalies in bulk properties at T_0 at ambient pressure¹¹. Therefore, the peculiarity of CeCoSi is considered to arise from the high T_0 under pressure. Ferroic quadrupolar orderings induce lattice distortion as a cooperative Jahn-Teller effect^{23,24}. Lattice instability, which can assist the ferroic quadrupole ordering, is

an issue to be investigated in CeCoSi. Note that some tetragonal compounds show lattice distortion to triclinic symmetry even without a significant contribution from f -electrons^{25,26}. From another perspective, a similarity with CeRh₂As₂ in the same space group should also be considered. These structures do not possess the local space-inversion symmetry of the Ce site. Theoretical studies on CeCoSi^{15,27} suggested that the staggered type of an interorbital antisymmetric spin-orbit interaction stabilized an $O_{x^2-y^2}$ -type antiferroic electric quadrupole ordering. It is an interesting issue to see how these spin-orbit interactions influence the ferroic quadrupolar interaction.

IV. CONCLUSION

In summary, we measured field-angle-controlled ⁵⁹Co NMR spectra to reveal the nature of the nonmagnetic ordered phase in CeCoSi, which possesses well-separated CEF levels with $\Delta = 125$ K. The splitting of the NMR peak was interpreted by the formation of domains, where the Ce dipole moments were induced in different directions according to the domains. These features enable the unusual field-driven domain selection of the nonmagnetic phase. Our results suggest that the nonmagnetic phase in CeCoSi includes a ferroic O_{zx} -type quadrupole ordering. The triclinic distortion observed by XRD and no clear anomaly in NMR at T_{s1} were consistent with $O_{zx} + O_{yz}$ -type ordering below T_{s1} . Our results demonstrate that a quadrupole ordering is possible in a tetragonal system with large CEF splitting, which is comparable to that of the prototype Ce-based compound CeCu₂Si₂. This suggests that quadrupole interactions can appear in other tetragonal systems or make a non-negligible contribution behind major magnetic interactions.

ACKNOWLEDGMENTS

The authors thank K. Hattori, T. Ishitobi, T. Matsumura, Y. Kawamura, M. Yatsushiro, S. Hayami, H. Hidaka, K. Ishida, Y. Kuramoto, and K. Fujiwara for their insightful discussions. This work was supported by a Grant-in-Aid for Scientific Research on Innovative Areas ‘‘J-Physics’’ (Grants No. 15H05882, No. 15H05885, No. JP18H04320, and No. JP18H04321), Grant No. JP18H03683 and a Grant-in-Aid for JSPS Research Fellow (Grant No. JP19J00336) from JSPS.

APPENDIX

A. ⁵⁹Co nuclear quadrupole resonance and electric field gradient

Nuclear quadrupole resonance (NQR) measurements were performed on CeCoSi to obtain information about the structural distortion below T_0 under zero field. The NQR Hamiltonian is

nian is

$$\mathcal{H}_Q = \frac{h\nu_Q}{6} \left[3I_z^2 - I(I+1) + \frac{\eta}{2} (I_+^2 + I_-^2) \right], \quad (4)$$

where I is the nuclear spin ($I = 7/2$ for ⁵⁹Co), ν_Q is the quadrupole frequency, η is the asymmetric parameter, and h is the Planck constant. The Hamiltonian is derived from the electric field gradient (EFG) V_{ij} , which is diagonalized so that $|V_{zz}| \geq |V_{yy}| \geq |V_{xx}|$. The quadrupole frequency ν_Q is obtained from the EFG along the maximum principal axis V_{zz} as follows:

$$\nu_Q = \frac{3}{2I(2I-1)} \frac{eV_{zz}Q}{h}, \quad (5)$$

where Q is the nuclear quadrupole moment and e is the elementary charge. The asymmetric parameter η is defined as

$$\eta \equiv \frac{V_{xx} - V_{yy}}{V_{zz}}, \quad (6)$$

which satisfies $0 \leq \eta \leq 1$.

The local symmetry at the nucleus is deduced from the NQR frequencies. The Co site in CeCoSi possesses $\bar{4}m2$ symmetry, ensuring $\eta = 0$ above T_0 . In this case, three resonant lines arise at frequencies $\nu_i = i\nu_Q$ ($i = 1, 2, \text{ and } 3$). If the four-fold symmetry is broken, η emerges, which modifies ν_i . They are given by

$$\nu_1 = \nu_Q \left(1 + \frac{109}{30} \eta^2 \right), \quad (7)$$

$$\nu_2 = \nu_Q \left(2 - \frac{17}{15} \eta^2 \right), \quad (8)$$

$$\nu_3 = \nu_Q \left(3 - \frac{3}{10} \eta^2 \right) \quad (9)$$

within the second-order perturbation with respect to the η term in Eq. (4). The lowest line ν_1 is the most sensitive to the emergence of η . Then, the ratio between the first and the second lines is given by

$$\frac{\nu_2}{\nu_1} = 2 - \frac{42}{5} \eta^2. \quad (10)$$

The value ν_2/ν_1 is 12 times more sensitive to η^2 than ν_3/ν_2 reported previously¹⁶.

Figure 5 shows the NQR spectra arising from ν_1 and ν_2 lines between 10 and 28 K. Figure 6 shows the experimental result η estimated from the ratio ν_2/ν_1 . No significant increase of η was detected at $T_0 = 12$ K, and $\eta < 0.01$ was obtained as the upper limit. A small η persists above T_0 . A possible origin of this is the local inhomogeneity in the η term, which leads to the finite spacial average of η^2 even if the spacial average of η is zero in the tetragonal phase. Because the NQR frequency depends on η^2 , the local inhomogeneity could lead to the residual η as a background even in the tetragonal phase.

The EFG parameters are obtained by band calculation through a full-potential linear augmented plane wave (LAPW) calculation within the local density approximation (LDA).

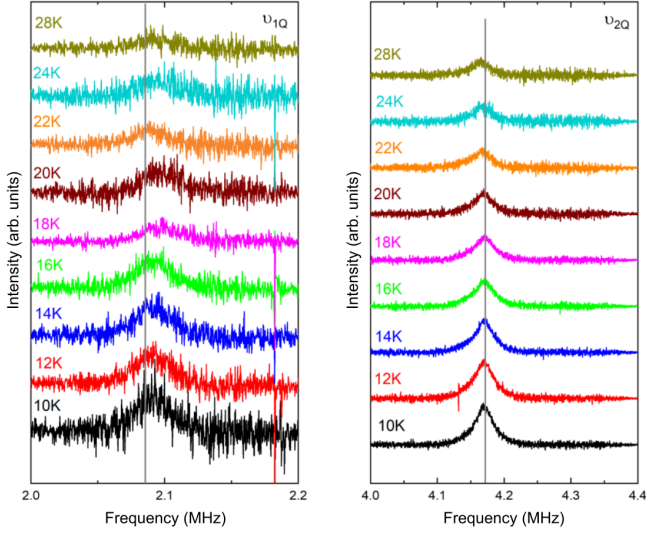


FIG. 5. Temperature dependence of the NQR ν_1 (left) and ν_2 (right) spectra. The spectra are shifted vertically. The solid lines indicate the case of $\eta = 0$ for $T = 10$ K.

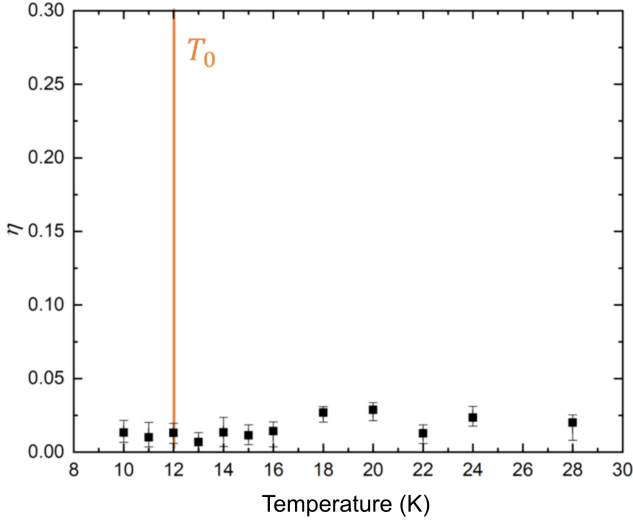


FIG. 6. Temperature dependence of the asymmetry parameter η estimated from the NQR ν_1 and ν_2 frequencies.

TABLE I. The quadrupole frequency ν_Q , asymmetric parameter η , and the angle θ_{zz} between the maximum principal axis V_{zz} and the tetragonal [001] axis from the band calculation and the NQR experiment at the Co site in CeCoSi.

	ν_Q (MHz)	η	θ_{zz} (deg)
Calc. (triclinic at 10 K)	2.12	0.013	0.16
Calc. (tetragonal at 20 K)	2.11	0	0
Expt. (NQR at 10 K)	2.085	< 0.01	—

The lattice parameters are from Ref. 21. The results are summarized in Table I. The quadrupole frequency ν_Q was calculated using the quadrupole moment of $Q = 0.42 \times 10^{-28} \text{ m}^2$ for ^{59}Co (Ref. 28). The calculated ν_Q is in good agreement with the experimental one. The band calculation shows that the asymmetric parameter is $\eta = 0.013$ below T_0 , which was in the same order as the experimental upper limit. The calculation supports the result that the breaking of four fold symmetry was so small it caused a tiny change in η .

The tilting of the V_{zz} was also estimated from band calculation. The obtained value $\theta_{zz} = 0.16^\circ$ is much smaller than the experimental NMR split angle $\Delta\theta \sim 2-3^\circ$ at 10 K. Thus, the NMR anomaly cannot solely be explained by the change in the EFG caused by the structural distortion.

B. Hyperfine coupling between the Co nucleus and 4f electrons

The hyperfine field at the Co nucleus from the nearest neighbor Ce sites is expressed as follows:

$$H_{\text{hf}} = \sum_{i=1}^4 B_i \cdot m_i, \quad (11)$$

where B_i is the hyperfine coupling tensor between the Co nucleus and the i th site, and m_i is the magnetic moment of the i th site. To explain the NMR line split, the following coupling tensor with off-diagonal elements is introduced:

$$B_1 = \begin{pmatrix} B_{aa}^1 & \sim 0 & B_{ac}^1 \\ \sim 0 & B_{bb}^1 & \sim 0 \\ B_{ca}^1 & \sim 0 & B_{cc}^1 \end{pmatrix}. \quad (12)$$

The coupling tensors for the other sites are obtained by rotating B_1 with respect to the c axis. The Ce moments are parallel in the ferroic order, and the hyperfine field is expressed as follows:

$$H_{\text{hf}} = \begin{pmatrix} A_{aa} & \sim 0 & B_{ac}^1 - B_{ac}^2 \\ \sim 0 & A_{bb} & A_{ac}^4 - B_{ac}^3 \\ B_{ca}^1 - B_{ca}^2 & B_{ca}^4 - B_{ca}^3 & A_{cc} \end{pmatrix} \cdot m, \quad (13)$$

$$= Am, \quad (14)$$

where

$$A_{aa} \equiv B_{aa}^1 + B_{aa}^2 + B_{bb}^3 + B_{bb}^4, \quad (15)$$

$$A_{bb} \equiv B_{bb}^1 + B_{bb}^2 + B_{aa}^3 + B_{aa}^4, \quad (16)$$

$$A_{cc} \equiv B_{cc}^1 + B_{cc}^2 + B_{cc}^3 + B_{cc}^4. \quad (17)$$

The tilting of H_{total} is explained by an emergence of the induced field, H_{ind} , at the Co site, whose component is normal to H_{ext} . Since $H_{\text{ind}}/H_{\text{ext}} \approx \tan(\Delta\theta)$, the field-independent $\Delta\theta$ indicates that H_{ind} is proportional to H_{ext} . The Ce sites should be uniform even below T_0 , because the Co sites are uniform. When H_{ext} is along the [100] axis, the orthogonal H_{ind} at the

Co nucleus from the nearest neighbor Ce sites is expressed as follows:

$$H_{\text{ind}} = A_{cc}m_c + A_{ca}m_a, \quad (18)$$

where m_c and m_a are the [001] and [100] components of the Ce moment, and A_{cc} and A_{ca} are components the hyperfine coupling tensor. The angle $\Delta\theta \approx 2^\circ$ corresponds to

$H_{\text{ind}}/H_{\text{ext}} \approx \tan(\Delta\theta) \approx 3.5\%$, which is comparable to the in-plane Knight shift $K_{aa} = A_{aa}m_a/H_{\text{ext}} \approx 3.6\%$ at 12 K¹⁶. It is less likely that the off-diagonal component A_{ca} , which was zero in tetragonal symmetry¹⁶, is comparable to the diagonal part A_{aa} . H_{ind} is thought to be dominated by the perpendicular moment $A_{cc}m_c^c$. Similarly, when the field is along the [001] axis, the induced moment m_{ind}^a causes the induced field $A_{aa}m_{\text{ind}}^a$ at the Co site.

-
- * manago@riko.shimane-u.ac.jp
- ¹ H. Yamauchi, H. Onodera, K. Ohoyama, T. Onimaru, M. Kosaka, M. Ohashi, and Y. Yamaguchi, *J. Phys. Soc. Jpn.* **68**, 2057 (1999).
 - ² H. S. Jeevan, C. Geibel, and Z. Hossain, *Phys. Rev. B* **73**, 020407(R) (2006).
 - ³ P. Morin and J. Rouchy, *Phys. Rev. B* **48**, 256 (1993).
 - ⁴ M. Kosaka, H. Onodera, K. Ohoyama, M. Ohashi, Y. Yamaguchi, S. Nakamura, T. Goto, H. Kobayashi, and S. Ikeda, *Phys. Rev. B* **58**, 6339 (1998).
 - ⁵ J. Gaudet, E. M. Smith, J. Dudemaine, J. Beare, C. R. C. Buhariwalla, N. P. Butch, M. B. Stone, A. I. Kolesnikov, G. Xu, D. R. Yahne, K. A. Ross, C. A. Marjerrison, J. D. Garrett, G. M. Luke, A. D. Bianchi, and B. D. Gaulin, *Phys. Rev. Lett.* **122**, 187201 (2019).
 - ⁶ R. Sibille, N. Gauthier, E. Lhotel, V. Porée, V. Pomjakushin, R. A. Ewings, T. G. Perring, J. Ollivier, A. Wildes, T. C. Ritter, Clemens Hansen, D. A. Keen, G. J. Nilsen, L. Keller, S. Petit, and T. Fennell, *Nat. Phys.* **16**, 546 (2020).
 - ⁷ Y. Kawarasaki, T. Matsumura, M. Sera, and A. Ochiai, *J. Phys. Soc. Jpn.* **80**, 023713 (2011).
 - ⁸ S. Khim, J. F. Landaeta, J. Banda, N. Bannor, M. Brando, P. M. R. Brydon, D. Hafner, R. K uchler, R. Cardoso-Gil, U. Stockert, A. P. Mackenzie, D. F. Agterberg, C. Geibel, and E. Hassinger, *Science* **373**, 1012 (2021).
 - ⁹ D. Hafner, P. Khanenko, E.-O. Eljaouhari, R. K uchler, J. Banda, N. Bannor, T. L uhmann, J. F. Landaeta, S. Mishra, I. Sheikin, E. Hassinger, S. Khim, C. Geibel, G. Zwicknagl, and M. Brando, *Phys. Rev. X* **12**, 011023 (2022).
 - ¹⁰ H. Tanida, Y. Muro, and T. Matsumura, *J. Phys. Soc. Jpn.* **87**, 023705 (2018).
 - ¹¹ H. Tanida, K. Mitsumoto, Y. Muro, T. Fukuhara, Y. Kawamura, A. Kondo, K. Kindo, Y. Matsumoto, T. Namiki, T. Kuwai, and T. Matsumura, *J. Phys. Soc. Jpn.* **88**, 054716 (2019).
 - ¹² E. Lengyel, M. Nicklas, N. Caroca-Canales, and C. Geibel, *Phys. Rev. B* **88**, 155137 (2013).
 - ¹³ S. E. Nikitin, D. G. Franco, J. Kwon, R. Bewley, A. Podlesnyak, A. Hoser, M. M. Koza, C. Geibel, and O. Stockert, *Phys. Rev. B* **101**, 214426 (2020).
 - ¹⁴ S. Horn, E. Holland-Moritz, M. Loewenhaupt, F. Steglich, H. Scheuer, A. Benoit, and J. Flouquet, *Phys. Rev. B* **23**, 3171 (1981).
 - ¹⁵ M. Yatsushiro and S. Hayami, *J. Phys. Soc. Jpn.* **89**, 013703 (2020).
 - ¹⁶ M. Manago, H. Kotegawa, H. Tou, H. Harima, and H. Tanida, *J. Phys. Soc. Jpn.* **90**, 023702 (2021).
 - ¹⁷ M. Takigawa, H. Yasuoka, T. Tanaka, and Y. Ishizawa, *J. Phys. Soc. Jpn.* **52**, 728 (1983).
 - ¹⁸ R. Shiina, H. Shiba, and P. Thalmeier, *J. Phys. Soc. Jpn.* **66**, 1741 (1997).
 - ¹⁹ Y. Tokunaga, Y. Homma, S. Kambe, D. Aoki, H. Sakai, E. Yamamoto, A. Nakamura, Y. Shiokawa, R. E. Walstedt, and H. Yasuoka, *Phys. Rev. Lett.* **94**, 137209 (2005).
 - ²⁰ T. Taniguchi, M. Yoshida, H. Takeda, M. Takigawa, M. Tsujimoto, A. Sakai, Y. Matsumoto, and S. Nakatsuji, *J. Phys. Soc. Jpn.* **85**, 113703 (2016).
 - ²¹ T. Matsumura, S. Kishida, M. Tsukagoshi, Y. Kawamura, H. Nakao, and H. Tanida, *J. Phys. Soc. Jpn.* **91**, 064704 (2022).
 - ²² H. Hidaka, S. Yanagiya, E. Hayasaka, Y. Kaneko, T. Yanagisawa, H. Tanida, and H. Amitsuka, *J. Phys. Soc. Jpn.* **91**, 094701 (2022).
 - ²³ P. Morin, J. Rouchy, and D. Schmitt, *Phys. Rev. B* **17**, 3684 (1978).
 - ²⁴ J. K. Kjems, H. R. Ott, S. M. Shapiro, and K. Andres, *J. Phys. Colloques* **39**, 1010 (1978).
 - ²⁵ J. Kitagawa and M. Ishikawa, *J. Phys. Soc. Jpn.* **68**, 2380 (1999).
 - ²⁶ P. Doleřal, M. Klicpera, J. Prchal, and P. Javorsk y, *Acta Phys. Pol. A* **127**, 219 (2015).
 - ²⁷ M. Yatsushiro and S. Hayami, *JPS Conf. Proc.* **30**, 011151 (2020).
 - ²⁸ N. Stone, *At. Data Nucl. Data Tables* **111-112**, 1 (2016).